

Head-on collision of viscous vortex rings

By S. STANAWAY¹, K. SHARIFF², AND F. HUSSAIN³

The head-on collision of two identical axisymmetric viscous vortex rings is studied through direct simulations of the incompressible Navier-Stokes equations. The initial vorticity distributions considered are those of Hill's spherical vortex and of rings with circular Gaussian cores, each at Reynolds numbers of about 350 and 1000. The Reynolds number is defined by Γ/ν , the ratio of circulation to viscosity. As the vortices approach each other by self-induction, the radii increase by mutual induction, and vorticity cancels through viscous cross-diffusion across the collision plane. Following contact, the vorticity distribution in the core forms a head-tail structure (for the cases considered here), a behavior which has also been observed in inviscid calculations (Shariff *et al.* 1988), 3D viscous calculations (Melander & Hussain 1988, MH), and experiments (Oshima 1978). The characteristic time of vorticity annihilation is compared with that of a 3D collision experiment (Schatzle 1987) and 3D numerical simulations (MH). It is found that the annihilation time is somewhat longer in our axisymmetric case than it is in the symmetry plane of the experiment and 3D numerical simulation. Furthermore, by comparing the annihilation time with a viscous timescale and a circulation timescale, we deduce that both the strain-rate due to local effects and that due to 3D vorticity realignment are important. The flow is computed to the large time Stokes flow limit where the circulation decays as $t^{-3/2}$ and the vorticity distribution agrees with the self-similar solution of the Stokes equations. In this limit, the self-annihilation is exactly twice the mutual annihilation. For one of the cases computed, the far-field quadrupole sound is compared with the experimental results of Kambe & Minota (1983). The agreement is quite good even though the two Re 's are very different.

1. Introduction

Organized vortex structures are seen in many turbulent flows (Cantwell 1981). Their interactions may involve a change in topology through reconnection. For example, trailing vortices of an aircraft cross link to form vortex rings (Crow 1970), or an elliptic jet may bifurcate by splitting of elliptic rings thus significantly enhancing mixing (Hussain & Husain 1987). This is an important process in turbulence since reconnection is likely to involve significant mixing, cascade of energy, dissipation, and helicity generation (Hussain 1986). Studying annihilation and reconnection may also benefit vortex filament methods which currently model such processes

1 NASA/Stanford Center for Turbulence Research

2 NASA Ames Research Center

3 University of Houston, Dept. of Mechanical Engineering

with *ad hoc* approaches (Leonard 1975). Another motivation for the study of reconnection is to determine its role in jet noise (Hussain 1983; Bridges & Hussain 1987).

Many vortex reconnection situations have been studied experimentally and numerically: two rings colliding at an angle (Schatzle 1987; Ashurst & Meiron 1987), two or more rings initially in the same plane (Oshima & Asaka 1977), hairpin vortex evolving into a vortex ring (Moin *et al.* 1986), and two sinusoidal vortex tubes of opposite circulations (MH, in this volume). For clarity of discussion, consider the case of MH shown in figure 1. As in all of the 3D situations, portions of the two vortices approach each other (figure 1a) and upon "contact" (figure 1b), vorticity is annihilated across the collision plane (plane yz). In 3D flow, annihilation is accompanied by vorticity realignment or *reconnection* (in the x direction). In contrast, an axisymmetric vortex ring collision (shown schematically in figure 2) contains only annihilation. It is useful, however, to consider annihilation alone since this process is kinematically related to reconnection. A cartoon of figure 1, shown by figure 3a, illustrates that because circulation is constant along vortex tubes, the rate-of-decrease of circulation in the *annihilating* region (plane xy) is equal to the rate-of-increase of circulation in the *connecting* region (plane yz). One objective of this work is to compute the annihilation time for the axisymmetric collision and compare this to experiments of rings colliding at an angle (Schatzle 1987) and to a numerical simulation of cross linking vortex tubes (MH) to determine the role of the three dimensionality of the vorticity field in annihilation.

More precisely, we are comparing the axisymmetric case to a plane in the 3D collision, specifically, to symmetry plane xy in figure 3. The vorticity contours in this plane, given by figures 4a-4d, correspond to figures 1a-1d. In the 3D problem the characteristics of the vorticity distribution affecting annihilation such as core size and shape, and the local radius of curvature of vortex filaments, referred to as *local effects*, are supplemented by non-local influences from the bridges which arise from vorticity realignment (for a discussion of bridging, see MH). The objective of this work is to quantify these local effects, which entirely compose the axisymmetric case, and determine their relevance to three dimensional reconnection.

2. Problem Description

The time-dependent annihilation of axisymmetric vortex rings is entirely governed by the local character of the vorticity (i.e. core shape, size, strength and curvature). General trends of this process can be understood by considering the velocity induced by these local effects, referred to as the *local induction* approximation (Batchelor 1973, p.510).

Because the domain is unbounded and does not contain any bodies, the only mechanism permitting the circulation of a vortex ring (i.e. defined by the circuit of figure 5) to change, is diffusion of vorticity across the axis of symmetry and the collision plane. We refer to diffusion across the symmetry axis as self annihilation, and across the collision plane as mutual annihilation. The rate-of-change of circulation

about a material circuit is given by

$$\frac{d\Gamma}{dt} = -\nu \oint (\nabla \times \omega) \cdot d\mathbf{l}. \quad (1)$$

Applying equation (1) to a quarter plane shown in figure 5 gives

$$\oint (\nabla \times \omega) \cdot d\mathbf{l} = \int_0^\infty \frac{1}{\sigma} \frac{\partial(\sigma\omega)}{\partial\sigma} dx - \int_\infty^0 \frac{\partial\omega}{\partial x} d\sigma \quad (2)$$

with the terms on the right hand side giving the contributions from segments 1 and 3 of figure 5; the contribution from segment 2 is zero. From this, we see that larger normal derivatives of vorticity along the x and σ axes result in greater rate-of-loss of circulation.

The effects that influence the gradients can be seen by the local induction approximation (Batchelor, p.519). Consider the induced velocity field resulting from line elements (length = $2L$) of two curved filaments (radius of curvature = R) which are in close proximity (separation distance = b) (figure 6). The induced velocity from a line element is resolved into its circumferential and binormal components. The circumferential component,

$$du_\phi(x, y) = \frac{\omega(x', y') dx' dy'}{2\pi\Delta}, \quad (3)$$

upon integration, represents the limit of a 2D vortex pair (i.e. dipole). Here, Δ is the distance between x, y and x', y' , the point where the line element intersects the xy plane. The binormal component,

$$du_b(x, y) = \frac{1}{4\pi R(x', y')} \omega(x', y') dx' dy' \log\left(\frac{L}{\Delta}\right) + \mathcal{O}(1) \quad (4)$$

gives the *self-induction* which presses the cores against each other and increases the gradients, and hence the circulation decay. Note that this analysis is valid only when b and the core size are much smaller than R and $2L$. The velocity field found from the integral of equation (3) causes the cores to translate and to subject each other to a strain rate that scales as $e \sim \Gamma/b^2$. As the cores approach, e increases.

Now for each instantaneous form of the velocity induced by one vortex on the other (characterized by e), there will be an equilibrium configuration in which the motion induced by one vortex on itself, is balanced by the flow induced by the other vortex. In other words if the self-induced motion were suppressed (thus fixing e) the locally two-dimensional flow would be steadily translating in the absence of viscosity. Such equilibrium shapes are well known and include a family of 2D translating pairs for uniform vorticity (Pierrehumbert 1980, among others) and the single solution for peaked vorticity (Batchelor 1973, p.535). If e changes slowly compared with the vorticity, adiabatic invariance will hold (Neu 1984, p.2400) and the cores will migrate through the equilibrium shapes as they approach each other.

In this case, core deformation will be modest. In the cases considered here, the cores flatten considerably more indicating a loss of adiabatic invariance. The parameter governing this, α , is the ratio of how fast ϵ changes compared to the time scale of internal rotation:

$$\alpha \sim \frac{\frac{d}{dt} \left(\frac{\epsilon}{\omega} \right)}{1/T_{\text{rot}}}, \quad (5)$$

or,

$$\alpha \sim \frac{\delta^3}{b^3} \frac{\delta}{R} \log \left(\frac{R}{\delta} \right). \quad (6)$$

Thus, given the same core size to separation ratio (δ/b), cores that are thin compared to the radius of curvature are more resistant to distortion. Equations (3) and (4) give the qualitative behavior of the core approach and flattening in the limiting case of thin cores.

For the head-on collision the combined circulation of the two rings is zero ($\Gamma = 0$), and the term proportional to $\log L$ from self-induction vanishes upon integration. Furthermore, since $\log \Delta$ is the Green's function for the streamfunction (say Ψ_{2D}) of the locally 2D flow, one obtains upon integration

$$u_b(x, y, t) = \frac{\Psi_{2D}(x, y, t)}{R}. \quad (7)$$

Now, given an equilibrium 2D flow at each instant, on each streamline of the vortex

$$\Psi_{2D} = \Psi_o(t) - V(t)x, \quad (8)$$

where $\Psi_o(t)$ is the value of the streamfunction on the streamline in a reference frame translating with the dipole at velocity $V(t)$. Since $\Psi_o(t)$ is a function that decreases as the cores come together, the first term in equation (8) provides a *rigid* motion of the cores towards each other with an ever decreasing velocity while the second term provides a linear flattening in x (Shariff 1988).

3. Review of Earlier Work in Axisymmetric Vortex Ring Collisions

The problem of the collision of two axisymmetric vortex rings is classical and is described in the very first paper dealing with vortex motion (Helmholtz 1858) where it is assumed that the fluid is inviscid, and the cores sufficiently thin that they do not deform. In 1893 Dyson considered the case of a constant vorticity distribution in a circular core, rotating as a solid body and assumed large separations compared to core size. He found that the cores unphysically overlap when the rings have stretched by an amount

$$\frac{R}{R_o} = 1.06 \left[\log \left(\frac{8R_o}{\delta_o} \right) - \frac{7}{4} \right]. \quad (9)$$

Shariff *et al.* (1988) numerically solved a 1D evolution equation for the shape of the core boundary to investigate deviations from Dyson's solution for small separations.

They found that until the time when the radius has stretched approximately twice as far as indicated in equation (9) (2.49 instead of 1.06) the cores deform very little and instead follow the shapes of the steady 2D translating pairs computed by Pierrehumbert (1980).

Oshima (1978) conducted a smoke visualization study with Re_D ranging between 133 and 1865, based on initial propagation speed and exit diameter. Her photographs will be presented for comparison. Kambe & Minota (1983) studied the acoustic wave radiated when two shock-tube generated rings ($Re_D = 42,000$) collide. We shall provide comparison with the quadrupole part of the measured acoustic far-field signal. Considering the widely different Reynolds numbers of the experiment and simulation, the agreement is surprising. Kambe & Minota also develop a simple model for the trajectory of the vortices and decay of circulation. The model is based on an exact 1D solution of the Navier-Stokes equations for two layers of vorticity of opposite signs that are pressed together by an externally imposed plane strain.

After the present work was completed it came to our attention that Kambe & Myo Oo (1984) have studied the axisymmetric collision with a finite difference method in a bounded domain at Reynolds numbers (Γ/ν) from 140–1400 which are comparable to those of the present study. Liu & Ting (1982) employed a finite-difference scheme with boundary conditions specified using far-field expansions. They consider a vortex ring collision with $\Gamma/\nu = 201$, a very small initial separation equal to 0.20 of the toroidal radius and a core radius of 0.05 times the toroidal radius. Results are presented for a short time during which the the rings have stretched to only $R/R_o = 1.6$.

4. Methods

The Navier-Stokes equations are solved in an unbounded domain using a spectral code developed by Stanaway, Cantwell & Spalart (1988). The method relies on divergence-free basis functions, with the result that continuity is inherently satisfied and the pressure does not appear in the working equations. In particular, the basis functions are composed of Legendre polynomials in the polar direction and Jacobi polynomials matched to an algebraic mapping of the radial coordinate. Time advancement is second order accurate, implicit for the linear terms (Adams Bashforth), and explicit for the nonlinear term (Crank-Nicolson). The code has been tested using a comprehensive set of diagnostics (rate of convergence, stability at high Reynolds numbers, conservation of impulse, rate of energy decay etc.).

Given the dynamic solution, the quadrupole part of the acoustic signal is computed using the theory of vortex sound developed by Möhring (1978). It assumes that the sound source is compact. This means that if u and l are characteristic velocity and lengths of a vortical region and c_o is the speed of sound of the undisturbed medium, then the wavelength $c_o l/u$ of the radiation should be much larger than l , or, the eddy Mach number $M = u/c_o \ll 1$. The final working expression for

the far-field acoustic pressure p is

$$\begin{aligned}
 p(\mathbf{x}, t) &= \frac{\rho_o}{c_o^2} \frac{x_i x_j}{|\mathbf{x}|^3} Q'''_{ij}(t_r), \\
 Q'''_{ij}(t) &= \frac{1}{12\pi} \frac{\partial^3}{\partial t^3} \int y_i (\mathbf{y} \times \boldsymbol{\omega})_j \, dy, \\
 t_r &= t - |\mathbf{x}|/c_o.
 \end{aligned}
 \tag{10}$$

The novelty and usefulness of this expression lies in the fact that it relates the far-field acoustic pressure directly to the unsteadiness of the incompressible vorticity field via the third derivative of its second moment. Equation (10) represents the quadrupole part of the signal; a more complete theory by Kambe & Minota (1983) shows that in the presence of viscosity there is also a monopole whose time behavior is proportional to the second time derivative of the kinetic energy. We restrict attention here to just the quadrupole. For the axisymmetric case, equation (10) becomes

$$\begin{aligned}
 p(r, \theta, t) &= \frac{\rho_o}{4rc_o^2} \left(\cos^2 \theta - \frac{1}{3} \right) Q'''(t - r/c_o), \\
 Q'''(r) &\equiv \int x \sigma^2 \omega(x, \sigma) \, dx d\sigma.
 \end{aligned}
 \tag{11}$$

5. Results

Results are presented in figures 7-10 for initial conditions of thin and thick core rings at low and high Reynolds numbers. The parameters for each case are as follows:

CASE No. (FIGURE No.)	$(\Gamma/\nu)_o$	DESCRIPTION	PARAMETERS	
1 (7)	350	Thin core	$a_o/R_o = 0.35$	$X_o/R_o = 3$
2 (8)	1000	"	"	"
3 (9)	357	Smoothed Hill's vortex	$r_i = 0.8, r_o = 1.3$	$X_o/R_o = 2$
4 (10)	1073	"	"	"

For all of the cases shown, the resolution was fixed at 65×65 modes. For the thin core cases (1 & 2) the initial vorticity distributions in the cores are Gaussian (centered at X_o, R_o) with an "image" at $(X_o, -R_o)$ in order to ensure zero vorticity along the axis. The core radius, a_o , is defined as the distance from the center of the core to where the maximum velocity occurs in two-dimensions.

The initial vorticity profile for the thick core cases (3 & 4) is that of Hill's spherical vortex (Batchelor 1973 p.526). The abrupt jump in vorticity is replaced by a smooth transition between a specified inner radius, r_i , and an outer radius, r_o :

$$\omega = Ar \sin \theta \begin{cases} 1 & r \leq r_i \\ 1 - f(\xi) & r_i < r < r_o \\ 0 & r \geq r_o \end{cases}
 \tag{12}$$

where

$$f(\xi) = \exp[-K\xi^{-1} \exp(1/(\xi - 1))] \quad 0 \leq \xi \leq 1$$

$$\xi = \frac{r - r_i}{r_o - r_i} \quad K = 1/2(\exp 2)(\log 2).$$

following Melander *et al.* (1987).

For each of the cases presented, vorticity contours are shown at several instants (figures 7a-d, 8a-d, 9a-d, 10a-d), followed by time-dependent diagnostics. These instants (i.e. t_1, t_2, t_3, \dots) are marked on the curve, $\Gamma(t)$, by solid dots. Let us first consider the thin ring cases (figures 7 and 8). Driven by self-induction, the two vortex rings propagate toward each other. The core shapes begin to immediately adjust from the initial profile to a characteristic oblong shape shown by the vorticity contours of figures 7b and 8b. The peak vorticity, ω_p , initially decreases due to viscous diffusion (figures 7g, 8g) while the circulation remains constant (since a significant amount of vorticity has not yet reached either the collision plane or the axis of symmetry). The curve of ω_p is ragged because it is the maximum value of the vorticity on the grid points instead of the maximum value of the smooth function. As the rings get closer, the ring radii increase due to mutual induction, and neglecting viscosity this means that the vorticity of a vortex filament will increase like σ . These two effects are opposing each other, and their relative importance determines whether the peak vorticity will increase or decrease. For the high Re case (figure 8), stretching is more dominant as seen by the larger percentage increase of peak vorticity throughout the calculation. As the interaction proceeds, vorticity gradients steepen along the collision plane, and vorticity annihilation is enhanced. The cores do not continue to flatten uniformly but clump at the top forming a head-tail structure. Note that this head-tail structure is remarkably similar to figure 4 of the 3D collision. As the circulation decreases, mutual induction and stretching decrease and at some point, viscous diffusion dominates.

The stages are very similar for the Hill's vortex cases. One difference is that vorticity begins to annihilate across the axis of symmetry as the rings approach since the vorticity extends to the symmetry axis. From equation (2), we see the the vorticity will initially decay like

$$\left(\frac{d\Gamma}{dt}\right)_0 = -\frac{6\nu\Gamma_o}{R_H^2}, \tag{12}$$

where R_H is the radius of the vortex boundary. This behavior persists through t_2 in figure 9e and 10e.

Dissipation and rate-of-change of energy are plotted in figures 7f, 8f, 9f, 10f as solid and dashed lines, respectively. The curves of these two independently evaluated measures agree within plotting error, indicating that the viscous term is well resolved. The minima and maxima of the dissipation show very similar trends to ω_p in all of the cases.

The lower Re cases (figure 7, $Re = 350$ and figure 9, $Re = 357$) have essentially stopped stretching at the final time shown, while the higher Re cases (figure 8, $Re = 1000$ and figure 10, $Re = 1073$) are still stretching when the computation is stopped.

In the present version of the code, the rings are not able to be resolved for longer times than shown for figures 8 and 10. It is likely that the apparent oscillations in the tail in both cases are due to insufficient resolution. In future work, the code could either be tailored to compute this flow for longer times or run on a machine with more core memory than is allowed on the CRAY-XMP.

To summarize our observations, we define four phases of the collision of axisymmetric vortex rings: phase I – approach, where the only means of annihilation is diffusion across the axis of symmetry; phase II – collision and annihilation, where a characteristic head-tail structure is observed; phase III – arresting of vortex radius increase, where viscous diffusion dominates; phase IV – self-similar solution of the axisymmetric Stokes equations (i.e. the Stokes quadrupole solution).

The next issue is whether the annihilation time of the axisymmetric problem, t_{ann} , is of the same order as the circulation timescale, $T_c \equiv a_o^2/(\Gamma_o\nu)^{1/2}$, or the viscous timescale, $T_v \equiv a_o^2/\nu$ (note that $T_v = (\Gamma_o/\nu)^{1/2} T_c$). It was found in the symmetry plane of 3D problems (i.e. Schatzle 1987, and MH 1988) that the annihilation time was nearly equal to the circulation timescale. Furthermore, Schatzle suggested that out-of-plane strain enhances the rate of annihilation. Since the axisymmetric collision removes the out-of-plane strain while retaining the strain rate induced by local effects, a comparison of time scales is a first step in deducing the relative importance of the local and nonlocal effects.

The ratio of the annihilation time to circulation timescale in terms of the input parameters is

$$\frac{t_{\text{ann}}}{T_c} = \frac{\bar{t}_{\text{ann}}}{\bar{t}_o} \left(\frac{\Gamma_o}{\nu}\right)^{1/2} \left(\frac{R_o}{a_o}\right)^2 \frac{1}{\bar{R}_o} \quad (14)$$

where $\bar{R}_o = 3.0$, $\Gamma/\nu = 350$, $a_o/R_o = 0.25$, and from figure 7h, $\bar{t}_o = 1.0 \times 10^{-4}$, $\bar{t}_{\text{ann}} \approx 0.2 \times 10^{-4}$ (consult Stanaway (1988) for details of the normalization). Substituting these numbers into equation 14, we get $t_{\text{ann}}/T_c = 3.4$ and $t_{\text{ann}}/T_v = 0.18$. Therefore, the annihilation timescale for the axisymmetric collision is faster than the viscous timescale and slower than the timescale set by the circulation. This indicates the local effects are important in enhancing annihilation, however, nonlocal effects such as vorticity realignment are also important in 3D. In a 3D situation, one might expect that during the initial stages of the collision, local effects are dominant, and as the circulation in the symmetry plane weakens, the bridges strengthen and the out-of-plane strain becomes the more important effect.

To understand 3D effects on annihilation, consider for example, the simulation of MH. Those portions of the tubes that develop vorticity mainly in the x direction induce a strain that is out of the xy symmetry plane. If this induced flow could be modeled as an axisymmetric strain (radially inward in the xy plane and outward along z) then the effect on the locally two-dimensional solution is merely a rescaling of time and spatial coordinates. See for example Lundgren (1982, p.2194) who shows how one can generate an axially strained solution from a two-dimensional one. We do not yet have quantitative information about the type of strain present in the MH database, however, examination of the diagonal components of the strain-rate tensor in the detailed experimental measurements of Schatzle (1987) does suggest

axisymmetric strain in the symmetry plane at the location where the vorticity is the highest (From frame 16: pp. 114, 135, 142, 149 of his thesis). The non-locally induced flow can alter the sense of curvature of vortex lines through the xy section thus halting annihilation whereas in the axisymmetric case the curvature remains of one sign.

Another issue addressed with case 1 (figure 7) is the local contributions to annihilation and the final period of decay. The rate of change of circulation is shown in figure 7h with inlays of the vorticity distributions at particular times. Figures 7i, 7j, and 7k then show a plot of the integrand contributing to $\frac{d\Gamma}{dt}$ along the collision axis at three instants. Note that the tail does contribute significantly, indicating that a model of this process cannot neglect this region. Figure 7h shows the circulation on a log-log plot until very late times where it is seen to asymptote to $\Gamma \sim t^{-3/2}$. This behavior can be understood from a solution obtained by Phillips (1956) for the final period of decay of an inhomogeneous patch of turbulence. Basically the idea is to consider the evolution of the Fourier transform of the velocity expanded in the powers of the wavenumber κ . We write the expansion cryptically as

$$\hat{u} \sim I + (Q + A)\kappa + \dots \tag{15}$$

Here I and A are the conserved linear and angular impulse, respectively, both of which are zero in the present situation, and, Q is the quadrupole moment. At late times the nonlinear terms in the Navier-Stokes equation will be small and the high wavenumber parts of the transform will decay. Phillips shows that, to the extent that the nonlinear terms can be neglected, Q is constant. Hence at large times the only relevant parameters are Q and ν from which the behavior of Γ follows dimensionally. The explicit form for the quadrupole solution (Cantwell, private communication) is

$$\bar{\omega} = \frac{K}{\bar{t}^{5/2}} \eta^2 e^{-\eta^2} \sin(2\theta) \tag{16}$$

where $K = \text{constant}$, $\eta = \frac{r}{\sqrt{4\nu t}}$, $\bar{\omega} = \frac{\omega}{(I/\rho)}$, and θ is the polar angle (figure 2). The computed large time solution (figure 7k) is in agreement with this Stokes solution (equation 16). By substituting equation (16) into equation (2), it is found that for the asymptotic solution the contribution to circulation decay from the symmetry axis is exactly twice that from the collision line. In other words, in the asymptotic decay state, self-annihilation of the circulation is exactly twice mutual-annihilation.

Another issue studied with this case is that of noise generation. Kambe & Minota (1983) have measured the quadrupole part of the acoustic signal when high-speed rings ($Re_D = 42,000$) collide. Figure 12 compares the computed time factor $Q'''(t)$ (solid) with the measured value (dotted), the time origin being shifted to make the zero crossings coincide. The initial transient of the simulation is due to relaxation of the core shapes to equilibrium and may be remedied in the future by increasing the initial separation. The overall agreement at two widely different Re suggests that a certain integral measure of the two flows is insensitive to Re . Observing the relationship between the acoustic quadrupole, Q_{ij} , and Phillips' quadrupole

moment (for which he provides an evolution equation) we obtain

$$Q_{ij}'''(t) = 2\pi^2 \frac{d^2}{dt^2} \int (u_i u_j - 1/3 \delta_{ij} u^2) dx, \quad (17)$$

i.e. the strength and directivity of the quadrupole measures changes in the overall anisotropy of the velocity field and this appears to be insensitive to Re .

Figure 11 shows a comparison of the viscous calculation (case 4) with results obtained using the inviscid code of Shariff *et al.* (1988). The solid line is the boundary of the vortex across which ω/σ jumps from being constant to zero. The viscous vortices stretch less rapidly but in both cases the core shapes evolve similarly; they do not flatten uniformly but fill out and develop a tube-like head and a sheet-like tail similar to the 3D simulation of MH. The experimental photograph (figure 12a) from Oshima (1978) shows a similar structure. In the experiments the smoke in the head pinches and leaves the tail behind. This is shown in figure 12b which shows an oblique view at 30° from the plane of collision at a later instant. The inner disk is the tail and the outer circle is the head. The head-tail split is also clear in the MH simulation.

It is interesting that, in the inviscid calculation, while the head region at the final instant shown contains only 46% of the circulation, its self-energy is 88% of the total.

5. Conclusion

The head-tail structure has been observed in the viscous simulation of axisymmetric colliding vortex rings. Inviscid and viscous collision calculations show qualitatively the same head-tail core structure with the major difference that annihilation causes the vortex to slow down and to travel a finite distance. Among the time-dependent diagnostics computed were circulation, rate-of-change of energy, dissipation, peak vorticity, and impulse. The peaks in dissipation and maximum vorticity occur concurrently for all of the cases. The large time behavior was shown to be the quadrupole solution of the Stokes equations with the character that the self-annihilation due to diffusion of vorticity across the centerline of the vortex gives twice the annihilation as that of the vorticity across the collision plane in this limit. The time scale associated with one case was compared to the time scale observed in a 3D experiment and 3D simulation. It indicated that in 3D, both the out-of-plane strain and the strain-rate due to local effects are important.

Future work recommended includes increased resolution, further investigation of the noise generated at higher Reynolds numbers, and extension of these studies to three dimensions.

Acknowledgements

We would like to thank M.V. Melander for sharing with us his database and thoughts and P.R. Spalart for many useful discussions. F.H. gratefully acknowledges

support from the Center for Turbulence Research and ONR Grant N00014-87-K-0670.

REFERENCES

- ASHURST, W.T. & MEIRON, D.I. 1987 Numerical study of vortex reconnection. *Phys. Rev. Lett.* **58**, 1632–1635
- BATCHELOR, G.K. 1973 *An Introduction to Fluid Dynamics*. First paperback edition. Cambridge University Press.
- BRIDGES, J.E. & HUSSAIN F. 1987 Roles of initial condition and vortex pairing in jet noise. *J. Sound Vib.* **117**, 289–312.
- CANTWELL, B.J. 1981 Organized motion in turbulent flow. *Ann. Rev. Fluid Mech.* **13**, 457–515.
- CROW, S.C. 1970 Stability theory of a pair of trailing vortices. *A.I.A.A. J.* **8**, 2172–2179.
- DYSON, F.W. 1893 The potential of an anchor ring.— Part II. *Phil. Trans. Roy. Soc. London A* **184**, 1041–1106.
- HELMHOLTZ, H. VON 1858 On integrals of the hydrodynamical equations which express vortex motion. Transl. Tait, P.G., 1867 *Phil. Mag. Series 4* **33**, 485–512.
- HUSSAIN, A.K.M.F. 1983 Coherent Structures – Reality and Myth. *Phys. Fluids* **26**, 2816–2850.
- HUSSAIN, F. 1986 Coherent Structures and Turbulence. *J. Fluid Mech.* **173**, 303–356.
- HUSSAIN, F. & HUSAIN, H.S. 1987 Passive and active control of jet turbulence. In *Turbulence Management and Relaminarization* (ed. Liepman, H. & Narasimha, R.) Springer, 445–457.
- KAMBE, T. & MINOTA, T. 1983 Acoustic wave radiated by head-on collision of two vortex rings. *Proc. R. Soc. Lond. A* **386**, 277–308.
- LEONARD, A. 1975 Numerical simulation of interacting, three-dimensional vortex filaments. In *Fourth International Conference on Numerical Methods in Fluid Mechanics*, Springer, 245–250.
- LIU, C.H. & TING, L. 1982 Numerical solution of viscous flow in unbounded fluid. In *Eighth International Conference on Numerical Methods in Fluid Dynamics* (ed. Krause, E.) Lecture Notes in Physics **170**, Springer, 357–363.
- LUNDGREN, T.S. 1982 Strained spiral vortex model for turbulent fine structure. *Phys. Fluids* **25**, 2193–2203.
- MELANDER, M.V., MCWILLIAMS, J.C. & ZABUSKY, N.J. 1987 Axisymmetrization and vorticity gradient intensification of an isolated two-dimensional vortex through filamentation. *J. Fluid Mech.* **178**, 137–159.

- MELANDER, M.V. & HUSSAIN, F. 1988 Cut-and-connect of two antiparallel vortex tubes. In *CTR Proc. of the Summer Prog. 1988*.
- MÖHRING, W. 1978 On vortex sound at low Mach number. *J. Fluid Mech.* **85**, 685-691.
- MOIN, P., LEONARD, A., & KIM, J. 1986 Evolution of a curved vortex filament into a vortex ring. *Phys. Fluids* **29**, 995.
- MOORE, D.W. & SAFFMAN, P.G. 1975 The instability of a straight vortex filament in a strain field. *Proc. R. Soc. Lond. A.* **346**, 413-425.
- NEU, J. 1984 The dynamics of a columnar vortex in an imposed strain. *Phys. Fluids* **27**, 2397-2402.
- OSHIMA, Y. & ASAKA, S. 1977 Interaction of two vortex rings along parallel axes in air. *J. Phys. Soc. Jap.* **42**, 708-713.
- OSHIMA, Y. 1978 Head-on collision of two vortex rings. *J. Phys. Soc. Jap.* **44**, 328-331.
- PHILLIPS, O.M. 1956 The final period of decay of non-homogeneous turbulence. *Proc. Camb. Phil. Soc.* **52**, 135-151.
- PIERREHUMBERT, R.T. 1980 A family of steady, translating vortex pairs with distributed vorticity. *J. Fluid Mech.* **99**, 129-144.
- SADOVSKII, V.S. 1970 Vortex regions in a potential stream with a jump of Bernoulli's constant at the boundary. *Prikladnaia matematika i mekhanika* **35**, 729-735.
- SCHATZLE, P.R. 1987 An experimental study of fusion of vortex rings. Ph.D. Thesis, Graduate Aeronautical Laboratories, Caltech.
- SHARIFF, K., LEONARD, A., ZABUSKY, N., FERZIGER, J. 1988 Acoustics and dynamics of coaxial interacting vortex rings. *Fluid Dyn. Res.* **3**, 337-343.
- SHARIFF, K. 1988 Dynamics of a class of vortex rings. Ph.D. Thesis, Thermosciences division of Mechanical Eng. Dept., Stanford Univ. (to be submitted).
- SIGGIA, E.D. 1987 Vortex dynamics and the existence of solutions to the Navier-Stokes equations. *Phys. Fluids* **30**, 1606-1626.
- STANAWAY, S.K., CANTWELL, B.J. & SPALART, P.R. 1988 Navier-Stokes simulations of axisymmetric vortex rings. A.I.A.A. Paper 88-0318.
- STANAWAY, S.K. 1988 A numerical study of viscous vortex rings using a spectral method. Ph.D. Thesis, Aeronautics and Astronautics Dept., Stanford Univ., Also NASA TM 101041.

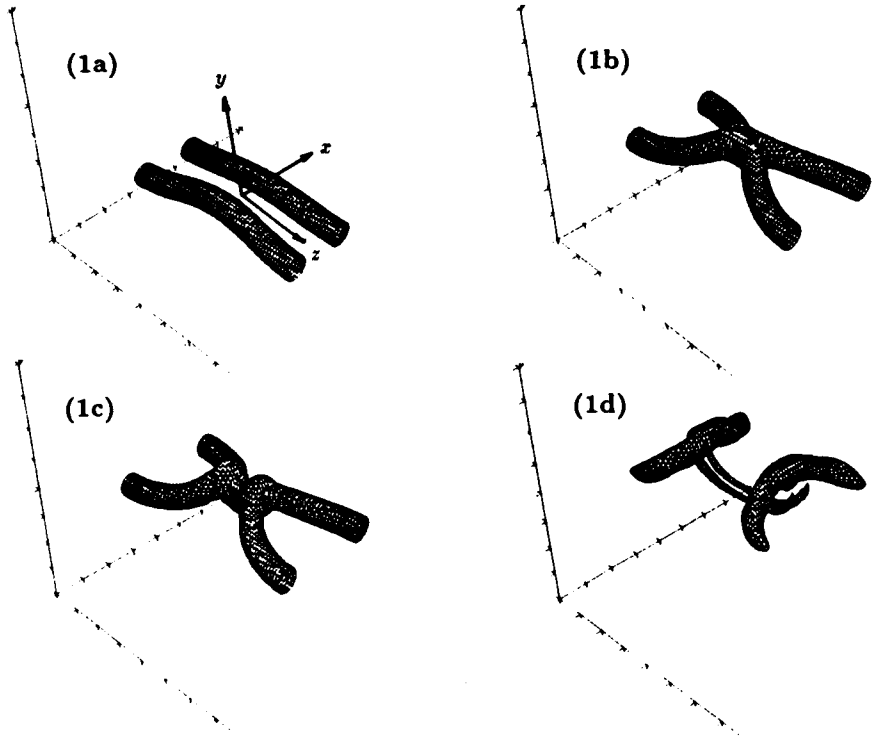


Figure 1. Numerical simulation of cross linking vortex tubes (figure courtesy of Melander & Hussain 1988). Surfaces correspond to a constant level of vorticity magnitude.

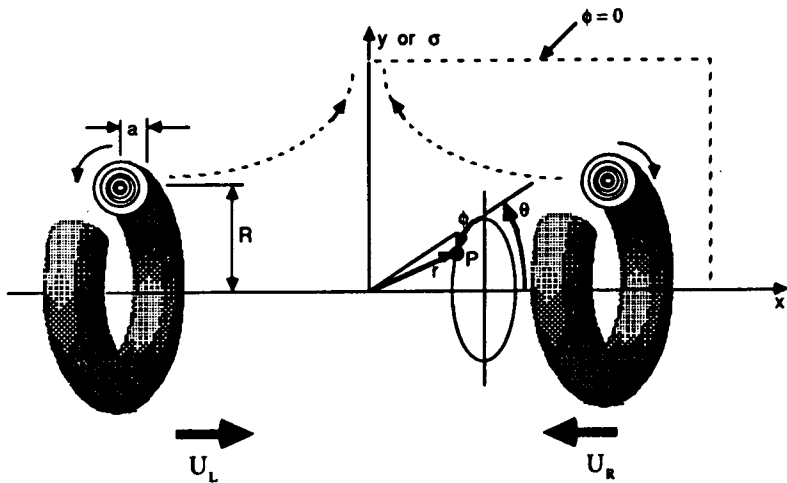


Figure 2. Schematic of axisymmetric vortex ring configuration used to study collision and annihilation.

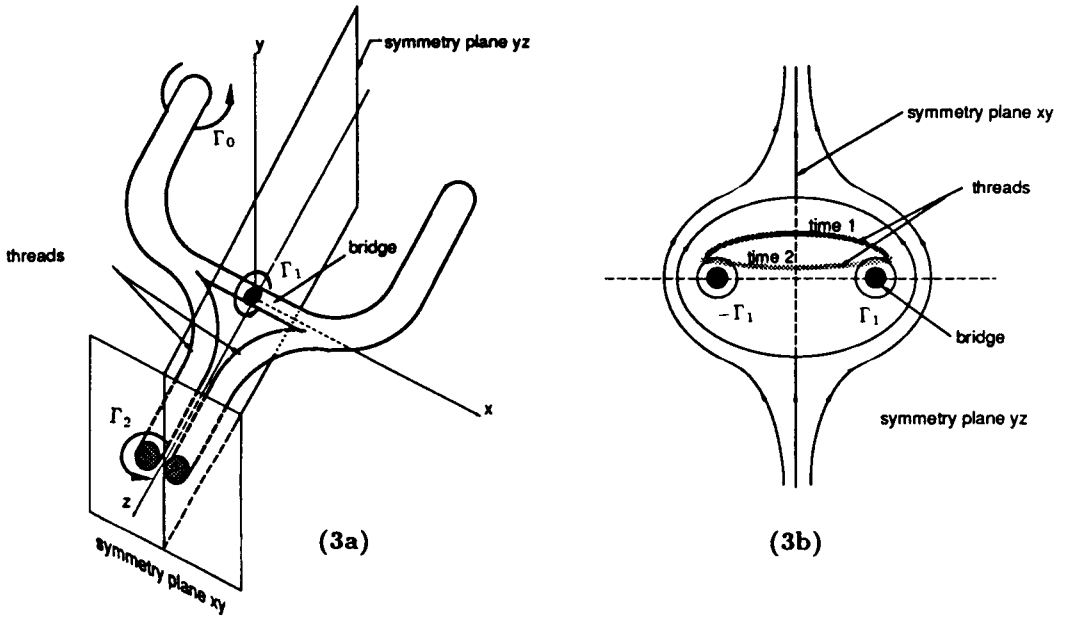


Figure 3. Schematic of cross linking vortex tubes (figure 1). (a) Showing bridges and threads. (b) Symmetry plane yz showing reversal of thread curvature from one time to the next.

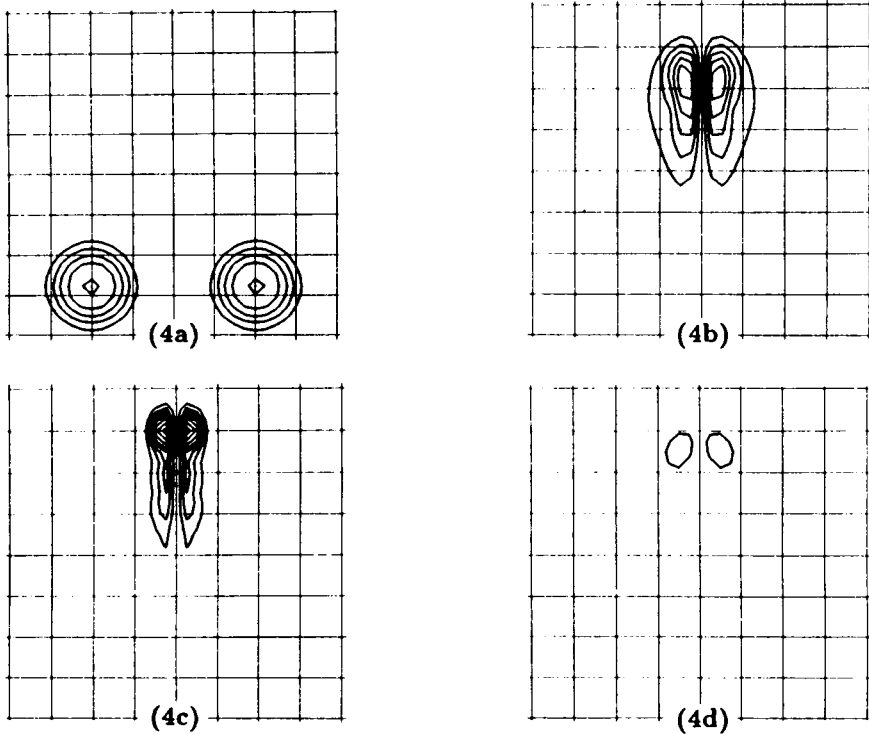


Figure 4. Vorticity contours in symmetry plane xy at times corresponding to figures 1a-1d (figure courtesy of Melander & Hussain 1988).

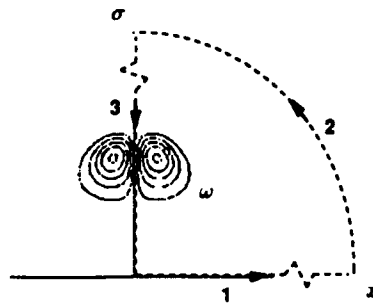


Figure 5. Schematic showing the definition of circulation in the collision of axisymmetric vortex rings of the same strength.

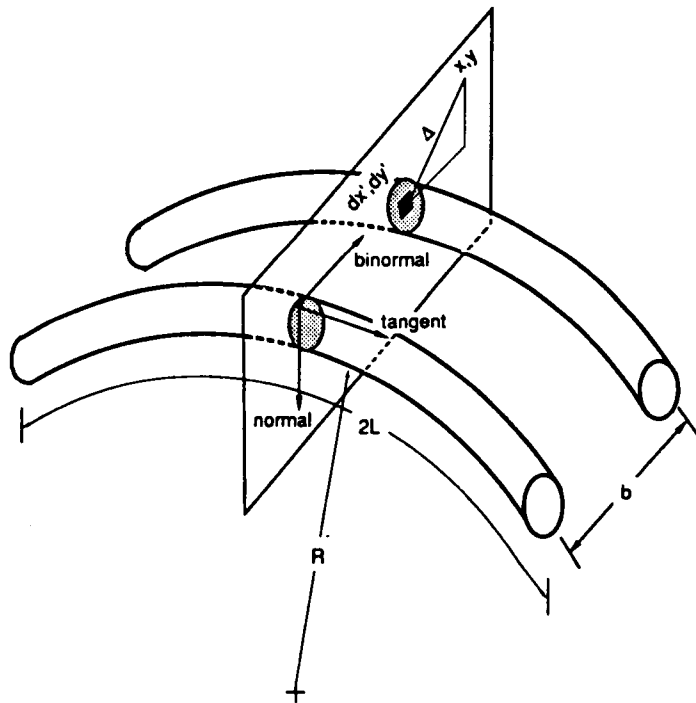


Figure 6. Local induction approximation of two curved vortex filaments of infinitesimal cross section.

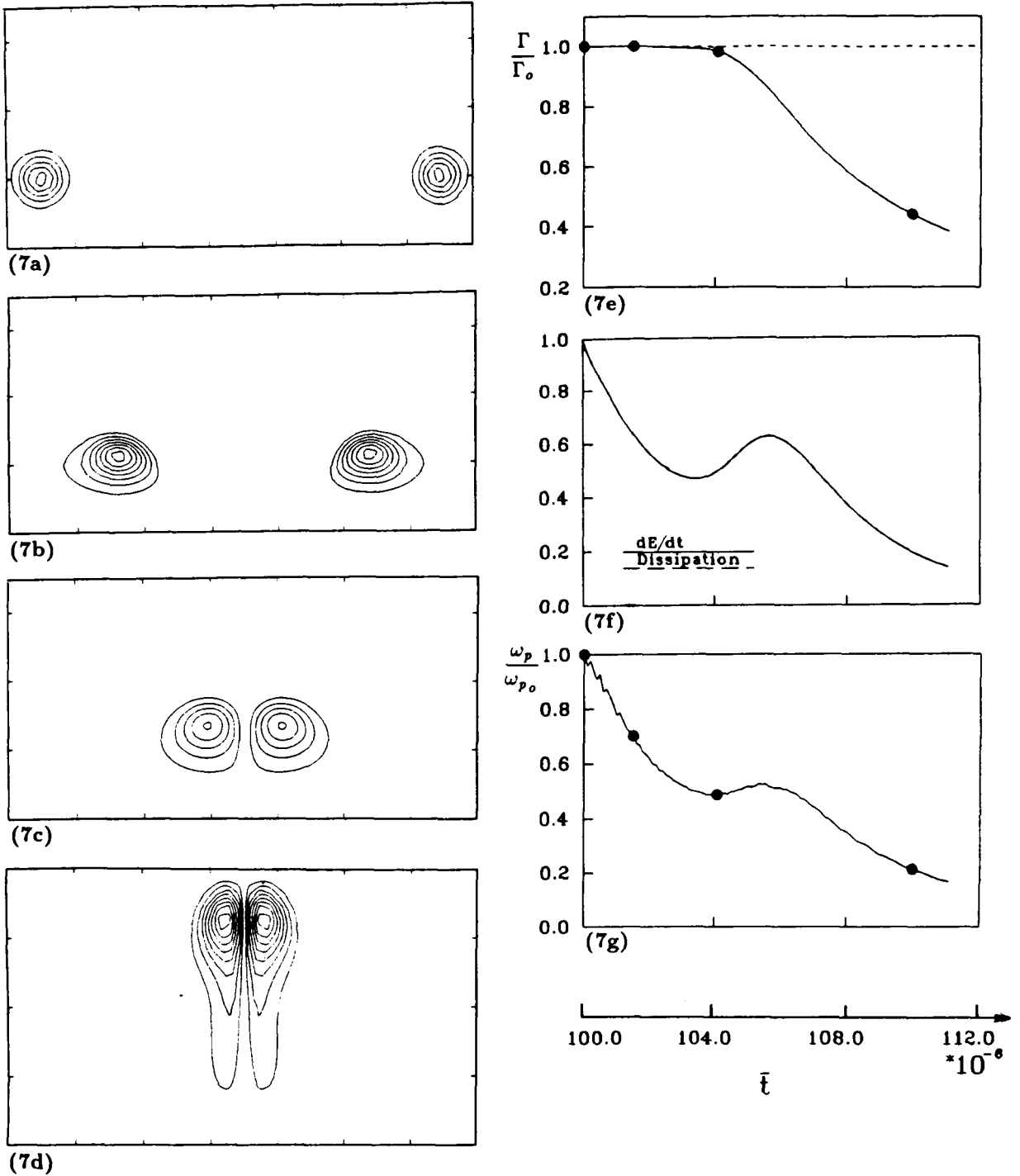


Figure 7. Axisymmetric collision, $(\Gamma/\nu)_0 = 350$, $(a/R)_0 = 0.35$: (a)-(d) vorticity contours; (e) circulation; (f) rate-of-change of energy and dissipation (relative to initial value); (g) peak vorticity (h) rate-of-change of circulation; (i)-(k) local contribution of vorticity annihilation along the collision plane; (l) log-log plot of circulation versus time; (m) time factor of the acoustic pressure.

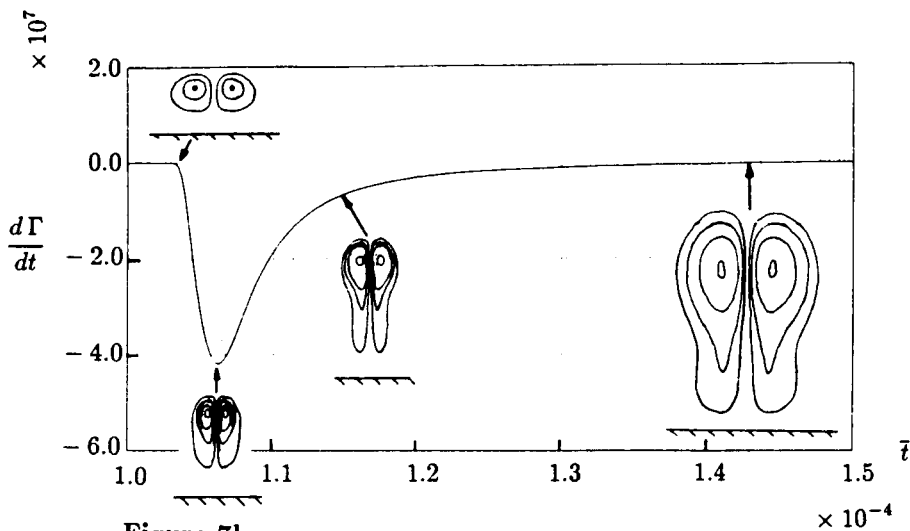


Figure 7h

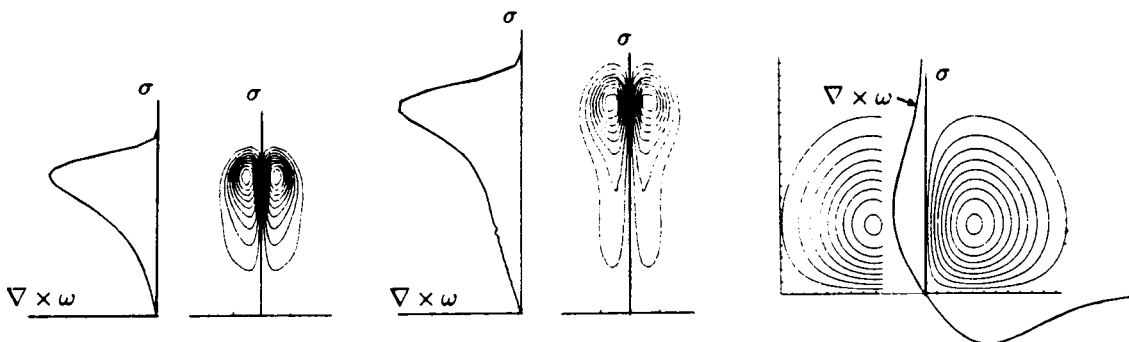


Figure 7i

Figure 7j

Figure 7k

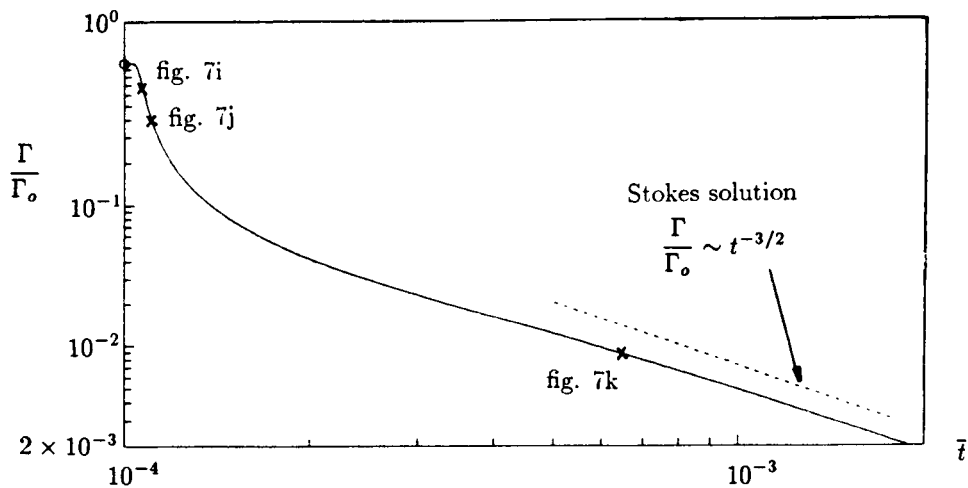


Figure 7l

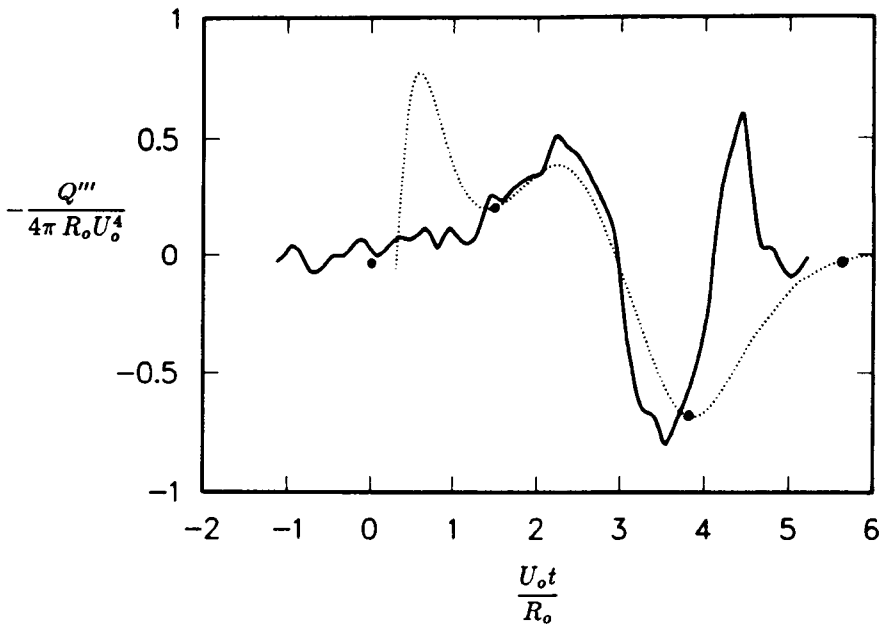


Figure 7m. Time factor of the acoustic pressure. \cdots Navier-Stokes simulation; $—$ experiment (Kambe & Minota 1983); \bullet instants corresponding to figures 7a-7d.

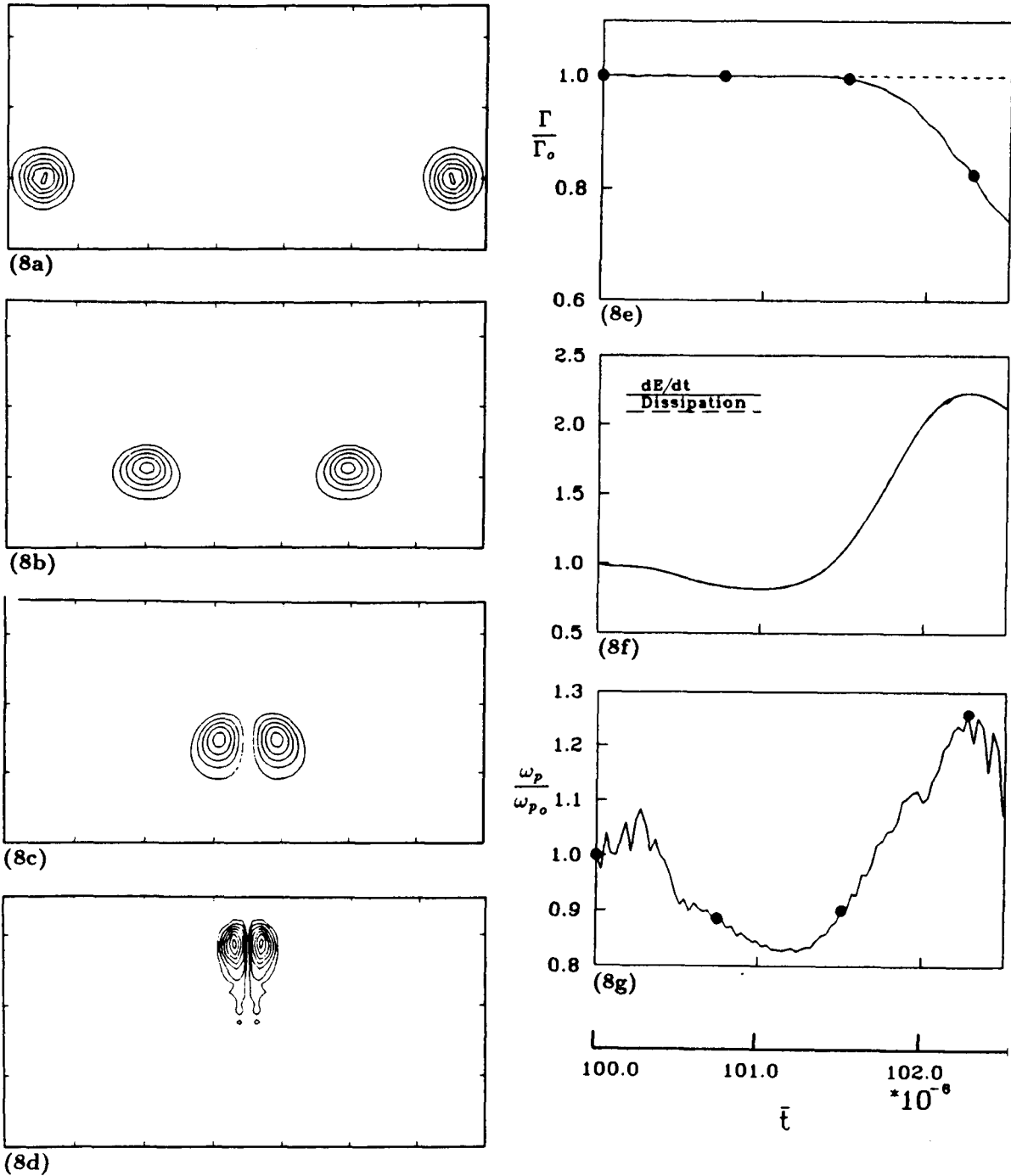


Figure 8. Axisymmetric collision, $(\Gamma/\nu)_0 = 1000$, $(a/R)_0 = 0.35$. (a)–(d) vorticity contours. (e) circulation (f) rate-of-change of energy and dissipation (relative to initial value); (g) peak vorticity.

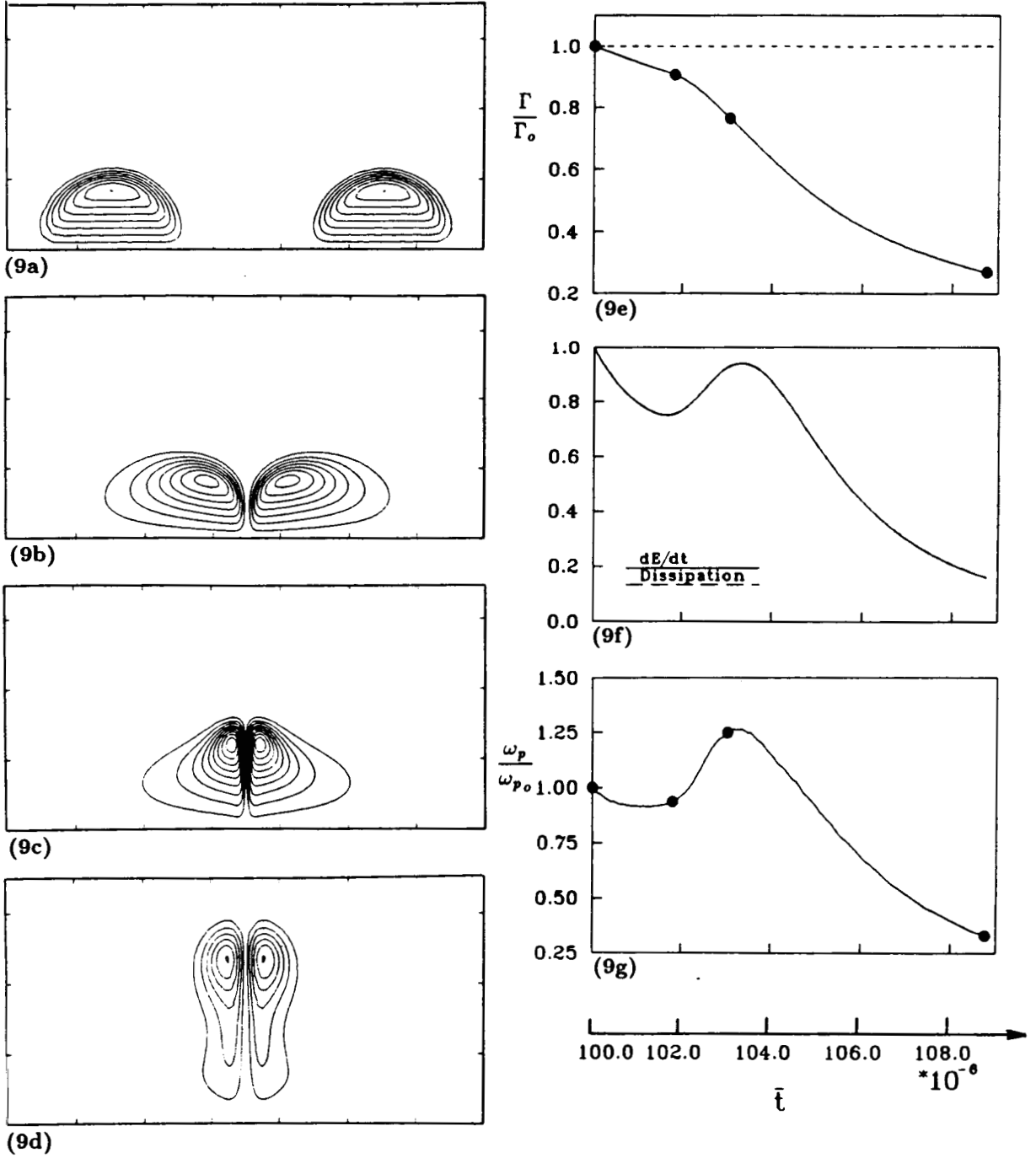


Figure 9. Axisymmetric collision, $(\Gamma/\nu)_0 = 357$, initial condition of Hill's spherical vortices. (a)–(d) vorticity contours. (e) circulation (f) rate-of-change of energy and dissipation (relative to initial value); (g) peak vorticity.

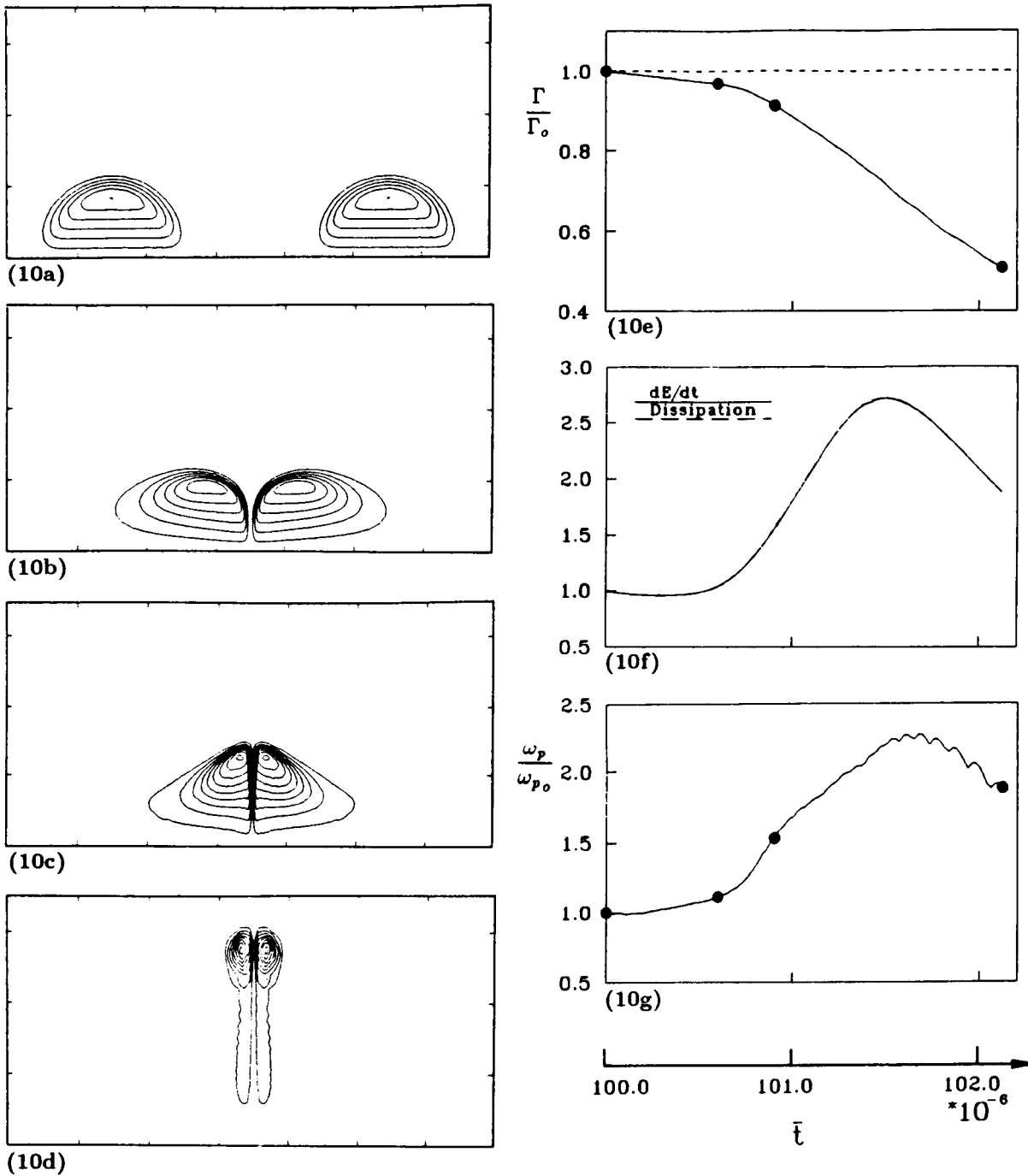


Figure 10. Axisymmetric collision, $(\Gamma/\nu)_0 = 1073$, initial condition of Hill's spherical vortices. (a)-(d) vorticity contours. (e) circulation (f) rate-of-change of energy and dissipation (relative to initial value); (g) peak vorticity.

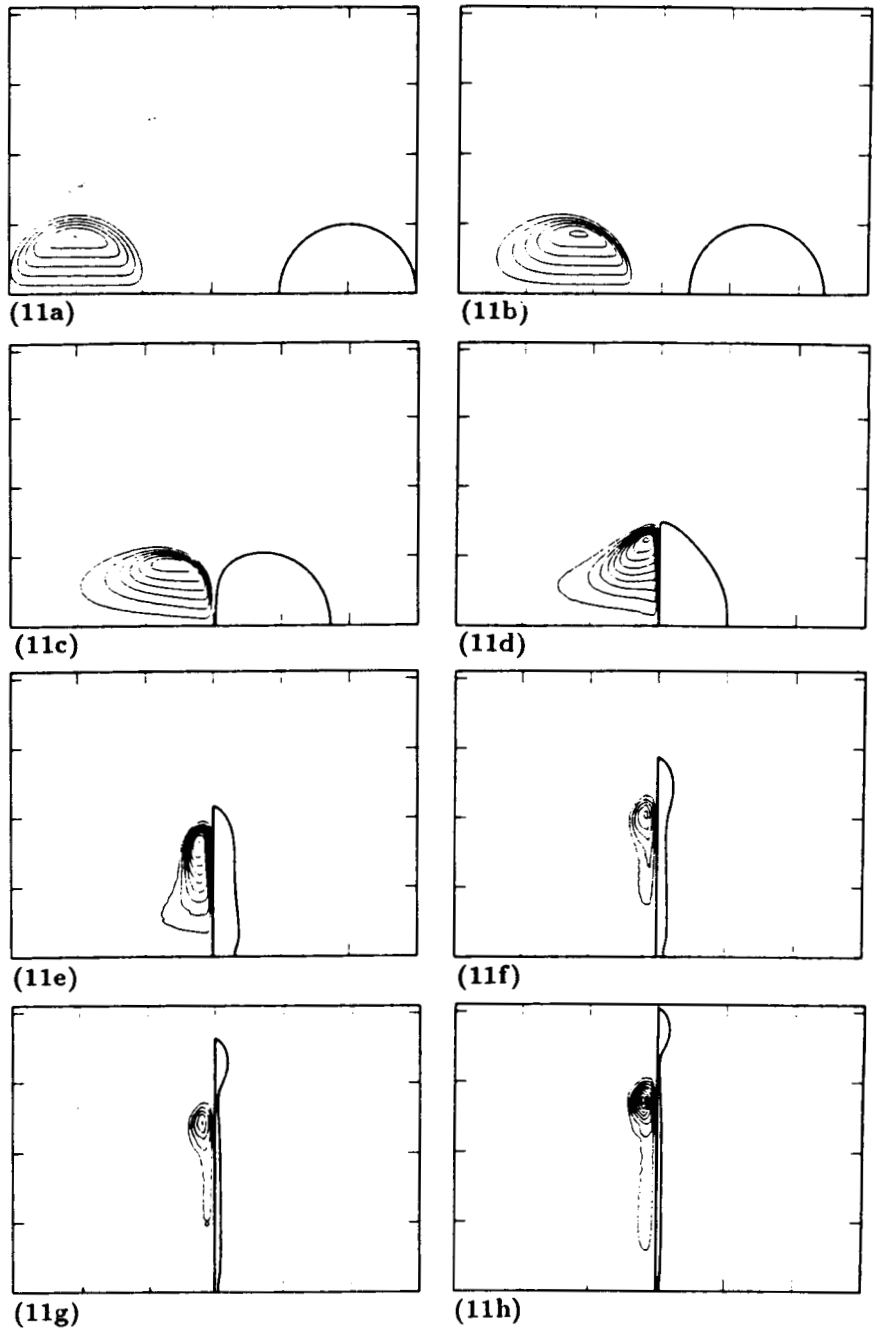


Figure 11. Comparison of viscous calculation of figure 10 (left half) and inviscid calculation using contour dynamics (right half).

ORIGINAL PAGE
BLACK AND WHITE PHOTOGRAPH

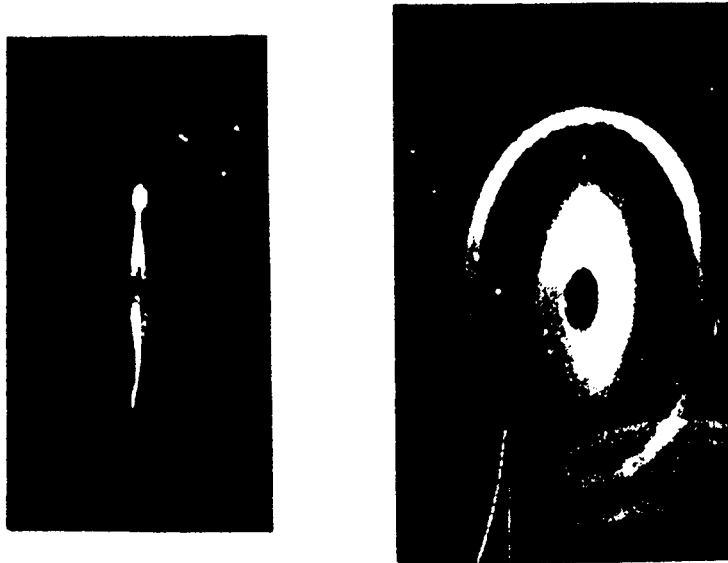


Figure 12. Experiment (Oshima 1978) showing core shape of colliding axisymmetric vortex rings: (a) side view; (b) oblique view at 30° from the plane of collision at a slightly later time.